D.V. Bandourin, V.F. Konoplyanikov, N.B. Skachkov

Jet energy scale setting with "$\gamma + Jet$" events at LHC energies. Detailed study of the background suppression.

1. INTRODUCTION

This paper continues our previous publications [1–4], where possibilities of jet energy scale setting and calibration of the hadron calorimeter at LHC energies by using "$\gamma + Jet$" process have been studied.

This article is devoted to the study of the background events suppression and to demonstration of the efficiency of the cuts introduced by us in paper [1] for this purpose.

2. ILLUSTRATION OF NEW CUTS EFFICIENCY

To estimate the background for the signal events, we have done the simulation [1] with a mixture of all QCD and SM subprocesses existing in PYTHIA with large cross sections, namely: ISUB=1, 2, 11–20, 28–31, 53, 68, which can lead to a big background for our main "signal" subprocesses (ISUB=14 and 29 in PYTHIA) [2]:

$$qg \rightarrow q + \gamma \tag{1a}$$

$$q\overline{q} \rightarrow g + \gamma \tag{1b}$$

Three generations (each of $50 \cdot 10^6$ events) with different values of minimal P_t of hard process $\hat{p}_\perp^{\,min}$ [3] have been done: the first one is with $\hat{p}_\perp^{\,min}$ = 40 GeV/c, while the second and the third – with $\hat{p}_\perp^{\,min}$ = 100 and 200 GeV/c, respectively.

We have selected "γ-candidate +1 Jet" events with ${P_t}^{jet} > 30\ GeV/c$ containing one γ-candidate to be identified by the detector as an isolated photon with ${P_t}^{\gamma} \geq 40$ (100 and 200) GeV/c for the generation with $\hat{p}_\perp^{\,min} \geq 40$ (100 and 200) GeV/c, respectively. One needs to stress that here and below, speaking about the γ-candidate, we imply in reality a signal that may be registered in the 3 by 3 ECAL crystal cell window with the highest P_t γ/e in the center. All these photon-candidates were supposed to satisfy the isolation criteria 1–4 of Section 3.2 from paper [1] with $P_{t\,CUT}^{isol} = 2\ GeV/c$ and $\epsilon_{CUT}^{\gamma} = 5\%$. No special cuts were imposed on $\Delta\phi$, ${P_t}^{out}$ and ${P_t}^{clust}$ (the values of ${P_t}^{clust}$ are automatically limited from the top since we select "γ-candidate +1 jet" events with ${P_t}^{Jet} > 30\ GeV/c$).

The corresponding distributions for the physical observables, introduced in Sections 3.1 and 3.2 from [1], are shown separately for the signal "γ - dir" and the background events in Figs. 1, 3, 5 and in scatter plots 2, 4, 6. First columns in these figures, denoted by "γ - dir", show the distributions in the signal events, i.e. in the events corresponding to the processes (1a) and (1b), having direct photons with ${P_t}^{\gamma-dir} \geq 40\ GeV/c$. The second columns, denoted as "γ - brem", correspond to the events in which the photons were emitted from quarks (i.e. bremsstrahlung photons) and have passed under the imposed cuts. The distributions in the third column were built basing on the events containing "γ-mes" photons, i.e. those photons that originate from multiphoton decays of mesons (π^0, η, ω, K_S^0) and have also passed under the imposed cuts.

Firstly we see that in the case of ${P_t}^{\gamma} \geq 200\ GeV/c$ (see Fig. 5) practically all "signal events" have $\Delta\phi < 15^\circ$, and in the case ${P_t}^{\gamma} \geq 100\ GeV/c$ (see Fig. 3) most of them are also

[1] PYTHIA 5.7 version with default CTEQ2L parametrisation of structure functions is used here.

[2] A contribution of another possible NLO channel $gg \rightarrow g\gamma$ (ISUB=115 in PYTHIA) was found to be still negligible even at LHC energies.

[3] CKIN(3) parameter in PYTHIA.

within $\Delta\phi < 15^\circ$. It is seen from Fig. 1 that at lower values ${P_t}^\gamma \geq 40\ GeV/c$ there is still a big number (about 70%) of the signal events belonging to the interval of $\Delta\phi < 15^\circ$. From here

we conclude that the upper cut $\Delta\phi < 15^\circ$ chosen in (26) of [1] is reasonable and indeed discards a lot of background events in all ${P_t}^\gamma$-intervals.

From the second "γ-brem" columns of Figs. 1, 3 and 5 one can also see that ${P_t}^{clust}$ spectra of the events with bremsstrahlung photons look quite different from the analogous ${P_t}^{clust}$ distributions of the signal "γ-dir" photons. The latter distributions have most of the events in the region of small ${P_t}^{clust}$ values.

Since the bremsstrahlung ("γ-brem") photons give the most sizable background, the found difference of the spectra prompts an idea of using a cut from the top on the value of ${P_t}^{clust}$ to reduce "γ-brem" background which dominates at large ${P_t}^{clust}$ values.

The analogous difference of ${P_t}^{out}$ spectra of signal "γ-dir" events (which also concentrate at low Pt^{out} values) from those of the background "γ-brem" and "γ-mes" events, with longer tails at high ${P_t}^{out}$ enables us to impose an upper cut on the ${P_t}^{out}$ value.

Now from the scatter plots in Figs. 2, 4 and 6 as well as from Figs. 1, 3 and 5 we can conclude that the usage of cuts (rather soft here, but their further restriction will be discussed below):

on $\Delta\phi$:

$$\begin{array}{lll} \Delta\phi < 15^\circ, & \text{for} & Pt^\gamma \geq\ 40\ GeV/c; \\ \Delta\phi < 10^\circ, & \text{for} & Pt^\gamma \geq 100\ GeV/c; \\ \Delta\phi <\ 5^\circ, & \text{for} & Pt^\gamma \geq 200\ GeV/c, \end{array}$$

on ${P_t}^{clust}$:

$$\begin{array}{lll} P_{t_{CUT}}^{clust} = 15\ GeV/c, & \text{for} & {P_t}^\gamma \geq\ 40\ GeV/c \ \text{ and } \ {P_t}^\gamma \geq 100\ GeV/c; \\ P_{t_{CUT}}^{clust} = 20\ GeV/c, & \text{for} & {P_t}^\gamma \geq 200\ GeV/c, \end{array}$$

on $P_{t_{CUT}}^{out}$:

$$\begin{array}{lll} P_{t_{CUT}}^{out} = 10\ GeV/c, & \text{for} & {P_t}^\gamma \geq\ 40\ GeV/c; \\ P_{t_{CUT}}^{out} = 15\ GeV/c, & \text{for} & {P_t}^\gamma \geq 100\ GeV/c \ \text{ and } \ {P_t}^\gamma \geq 200\ GeV/c \end{array}$$

would allow to keep the main part of the signal "γ-dir" events and to reduce noticeably the contribution from the background "γ-brem" and "γ-mes" events.

So, these figures evidently demonstrate how new physical variables ${P_t}^{clust}$ and ${P_t}^{out}$, introduced in Sections 3.1 and 3.2 of paper [1], can be useful for separation of "γ+Jet" events with direct photons from the background ones (as the latter, in principle, are not supposed to have good balanced ${P_t}^\gamma$ and ${P_t}^{Jet}$.

3. DETAILED STUDY OF BACKGROUND SUPPRESSION.

The study of this Section is based on the same sample of "signal + background" events ($50 \cdot 10^6$ for each interval of minimal P_t of the hard process: $\hat{p}_\perp^{min} = 40,\ 100,\ 200\ \ GeV/c$; see the beginning of Section 2) generated under the conditions described in the previous section and partially analyzed there. To demonstrate the way we have come to the final results, we

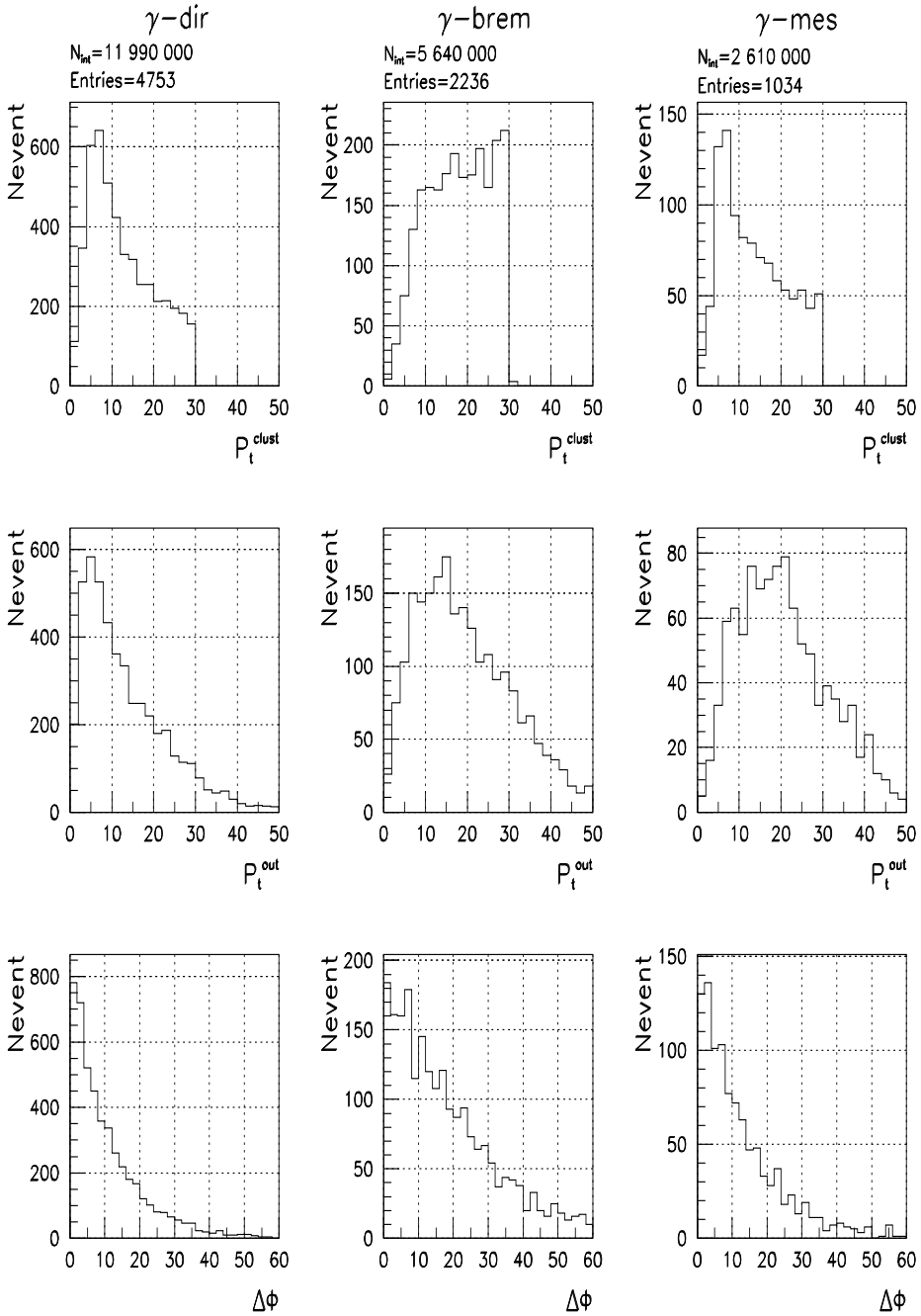

Fig. 1: Signal/Background: Number of events distribution over $P_t{}^{clust}$, $P_t{}^{out}$, $\Delta\phi$ ($P_t{}^{\gamma} \geq 40\ GeV/c$)

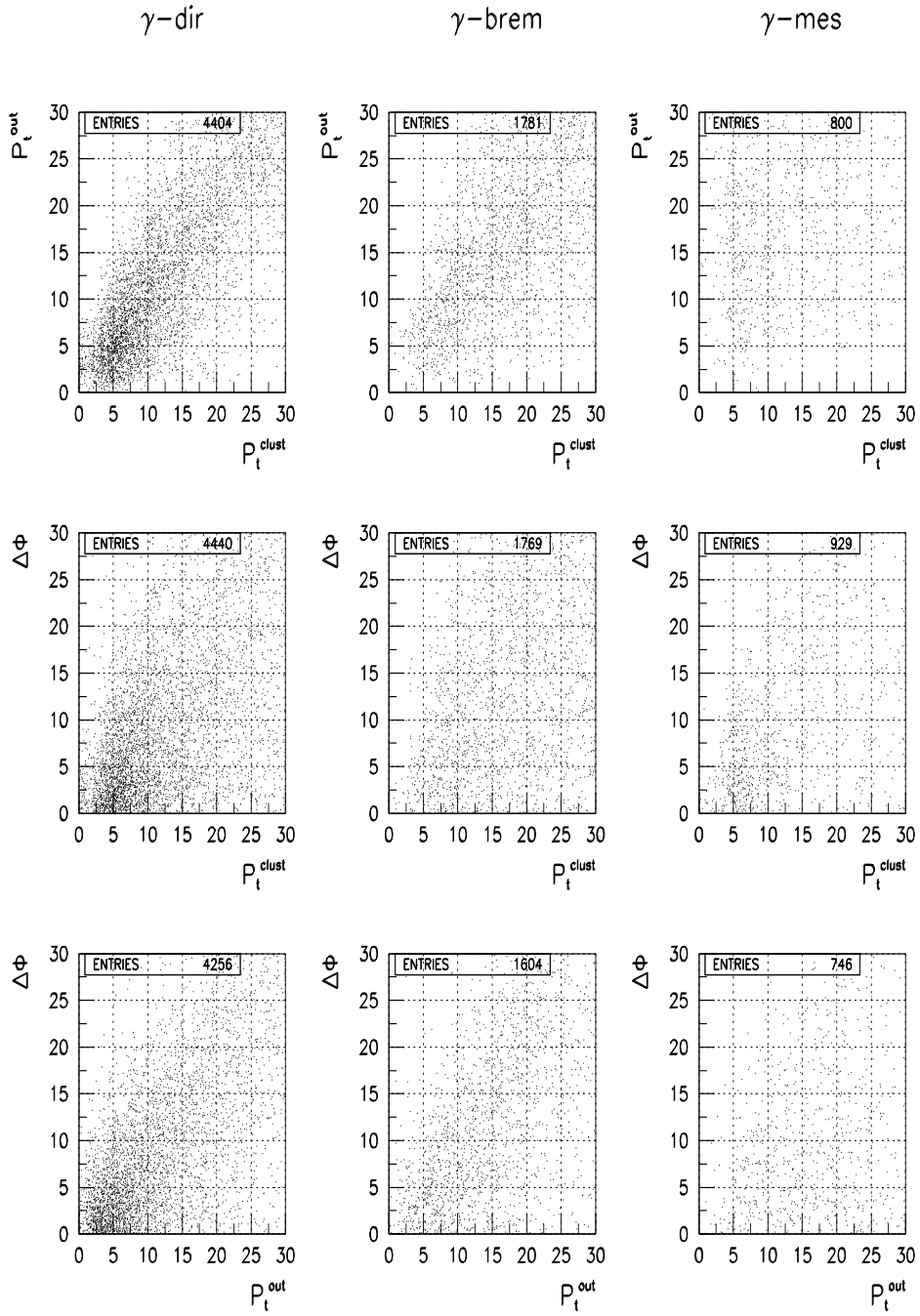

Fig. 2: Signal/Background: $P_t{}^{clust}$ vs. $P_t{}^{out}$, $P_t{}^{clust}$ vs.$\Delta\phi$, $P_t{}^{out}$ vs. $\Delta\phi$ ($P_t{}^{\gamma} \geq 40\,GeV/c$)

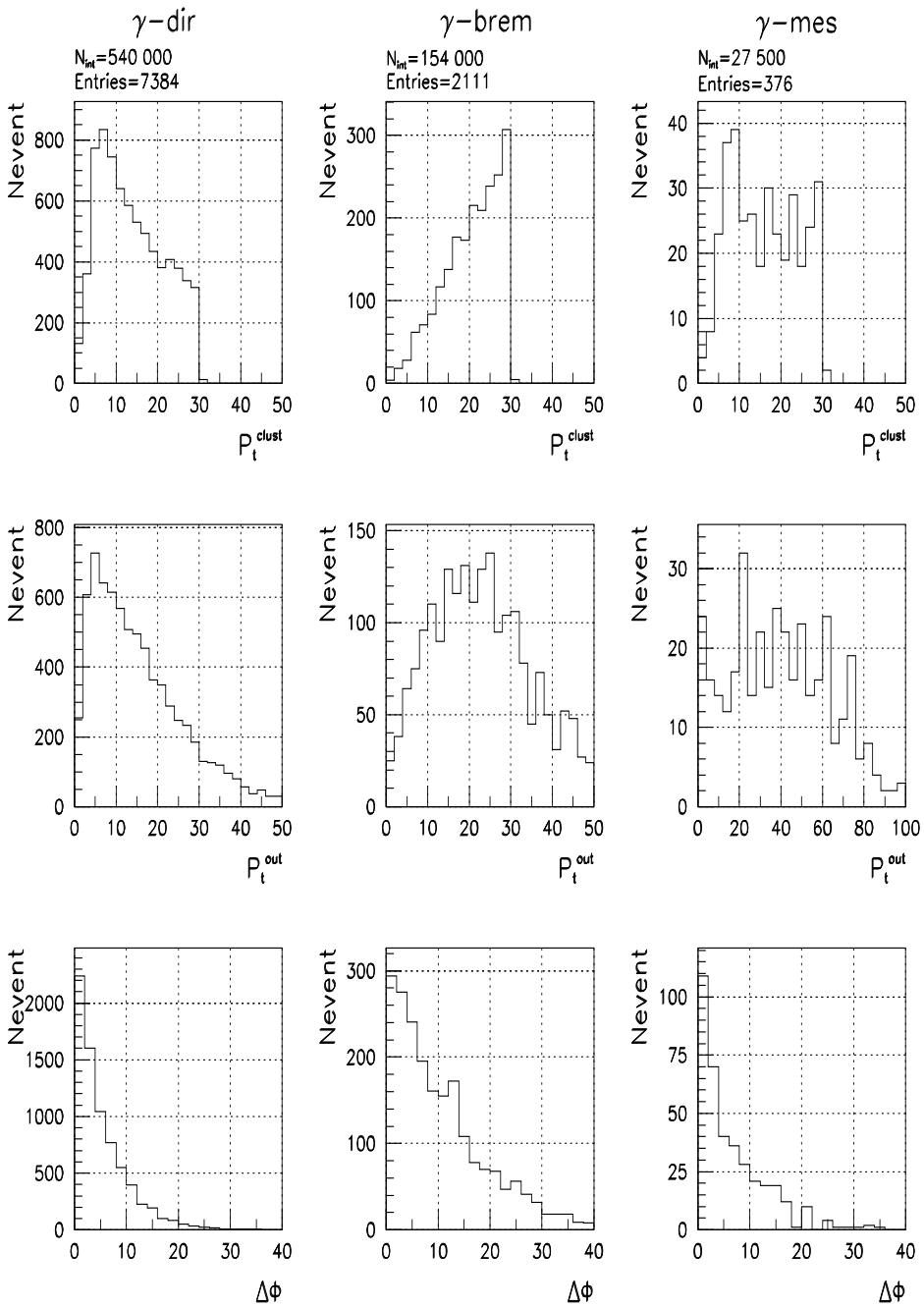

Fig. 3: Signal/Background: Number of events distribution over $P_t{}^{clust}$, $P_t{}^{out}$, $\Delta\phi$ ($P_t{}^{\gamma} \geq 100\ GeV/c$)

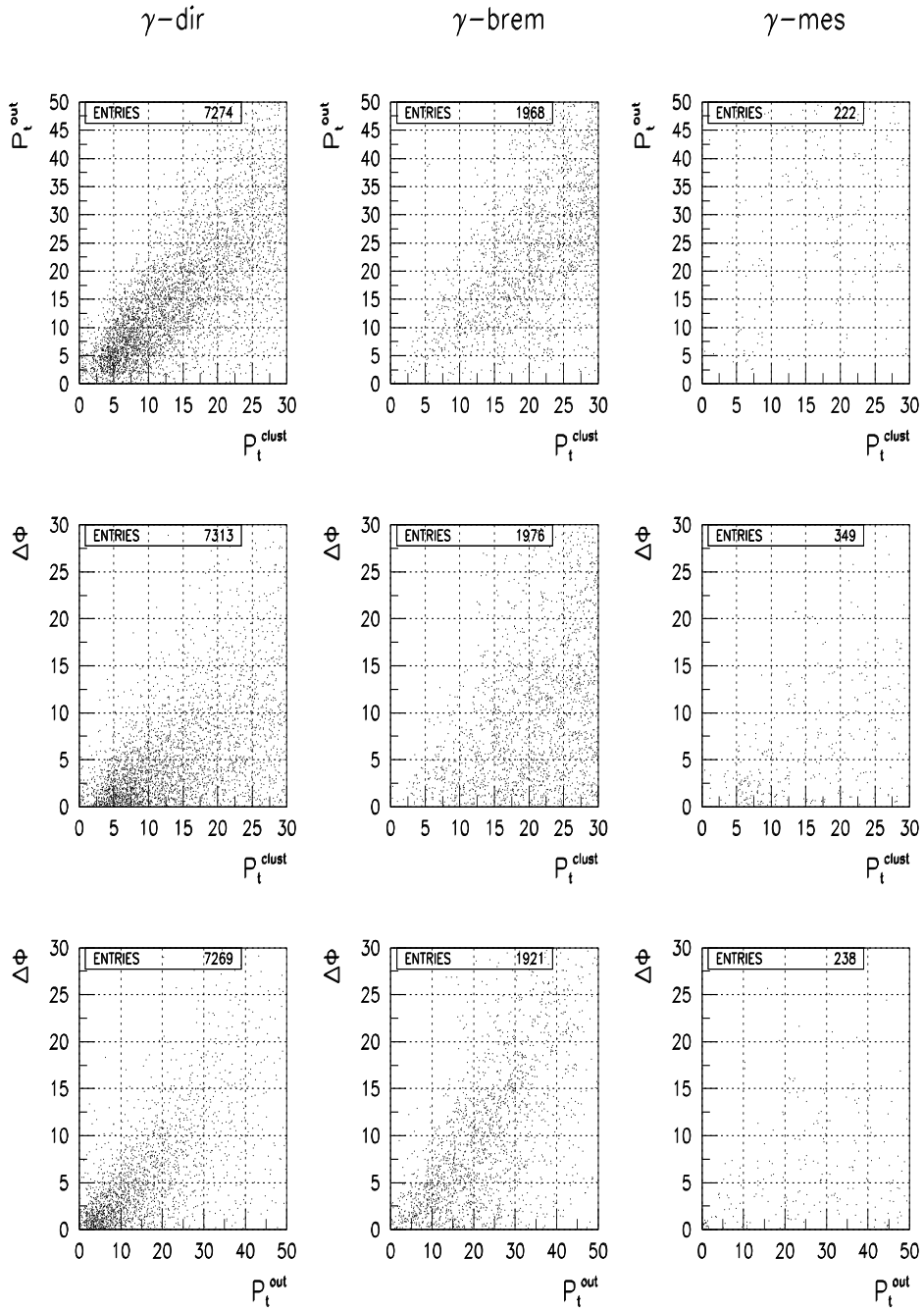

Fig. 4: Signal/Background: $P_t{}^{clust}$ vs. $P_t{}^{out}$, $P_t{}^{clust}$ vs.$\Delta\phi$, $P_t{}^{out}$ vs. $\Delta\phi$ ($P_t{}^{\gamma} \geq 100\ GeV/c$)

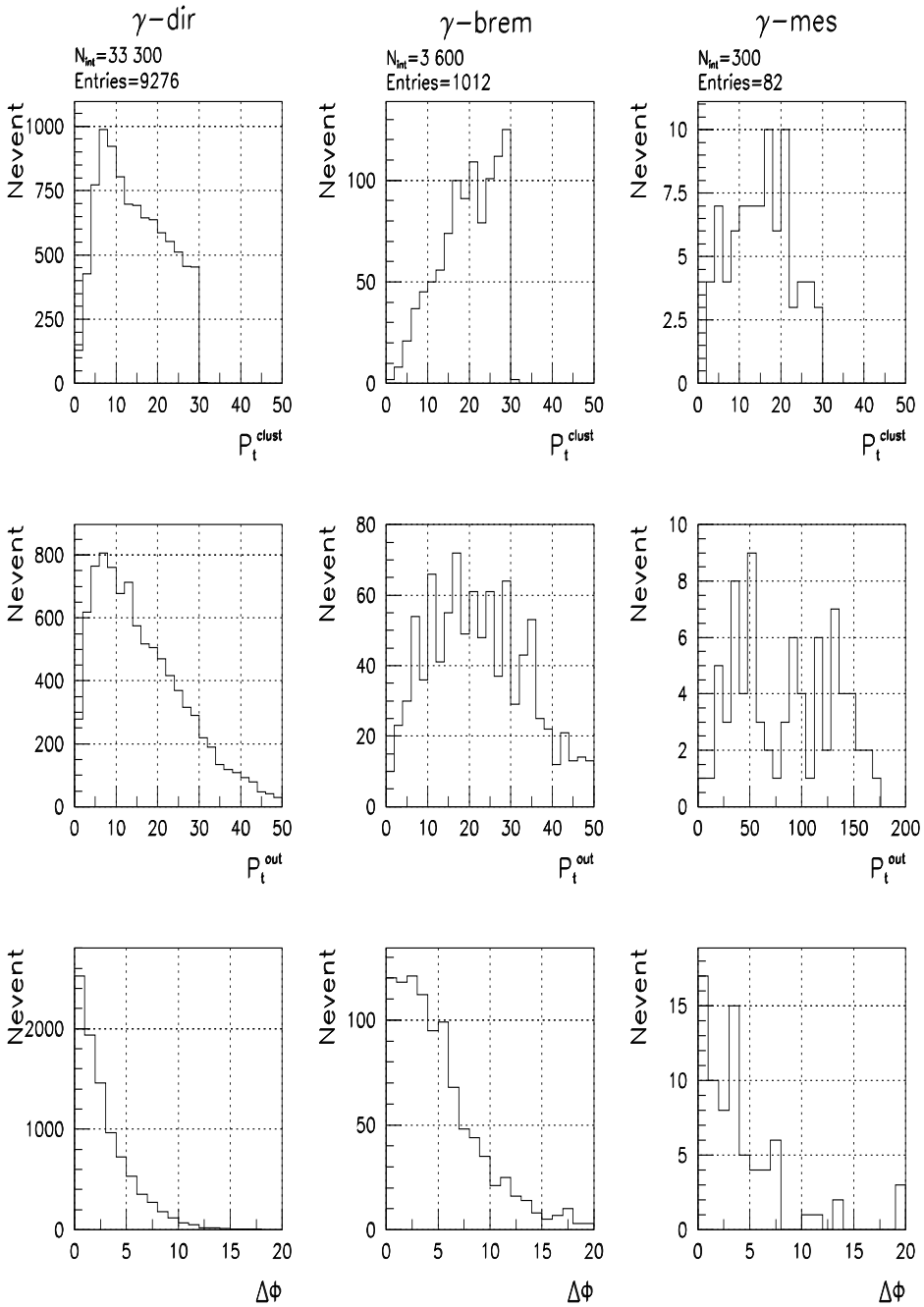

Fig. 5: Signal/Background: Number of events distribution over $P_t{}^{clust}$, $P_t{}^{out}$, $\Delta\phi$ ($P_t{}^{\gamma} \geq 200\ GeV/c$)

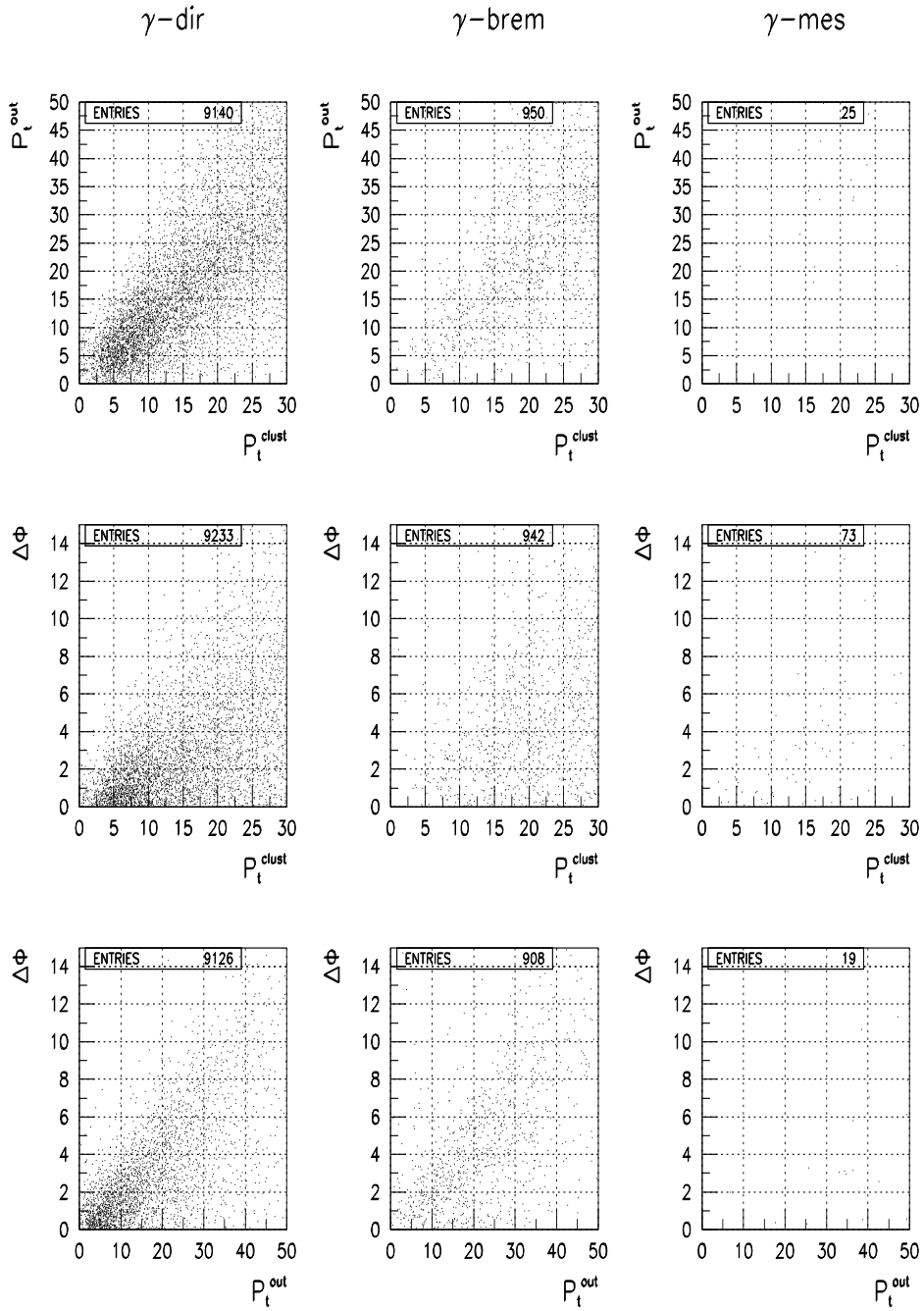

Fig. 6: Signal/Background: $P_t{}^{clust}$ vs. $P_t{}^{out}$, $P_t{}^{clust}$ vs.$\Delta\phi$, $P_t{}^{out}$ vs. $\Delta\phi$ ($P_t{}^{\gamma} \geq 200\ GeV/c$)

Table 1: List of the applied cuts used in Tables 2 – 5

0. No cuts;	
1. *a)* $P_t{}^{\gamma} \geq 40\ GeV/c$, *b)* $\lvert\eta^{\gamma}\rvert \leq 2.61$, *c)* $P_t{}^{jet} \geq 30\ GeV/c$, *d)* $P_t{}^{hadr} < 5\ GeV/c$ *;	
2. $\epsilon^{\gamma} \leq 15\%$;	**12**. $P_t{}^{clust} < 20\ GeV/c$;
3. $P_t{}^{\gamma} \geq \hat{p}_{\perp}^{\,min}$;	**13**. $P_t{}^{clust} < 15\ GeV/c$;
4. $P_t{}^{sum} < 1\ GeV/c$ ** ;	**14**. $P_t{}^{clust} < 10\ GeV/c$;
5. $\epsilon^{\gamma} \leq 5\%$	**15**. $P_t{}^{out} < 20\ GeV/c$;
6. $P_t{}^{isol} \leq 2\ GeV/c$;	**16**. $P_t{}^{out} < 15\ GeV/c$;
7. $Njet \leq 3$;	**17**. $P_t{}^{out} < P_{t\,CUT}^{out}$
8. $Njet \leq 2$;	$(P_{t\,CUT}^{out} = 10\ GeV/c$ for $\hat{p}_{\perp}^{\,min} = 100,\ 200\ GeV/c$
9. $Njet = 1$;	and $P_{t\,CUT}^{out} = 5\ GeV/c$ for $\hat{p}_{\perp}^{\,min} = 40\ GeV/c)$.
10. $\Delta\phi < 15^{\circ}$;	**18**. $\epsilon^{jet} \leq 5\%$;
11. $P_t{}^{miss} \leq 10\ GeV/c$;	**19**. $\epsilon^{jet} \leq 2\%$.

$*$ P_t of a hadron in the 5x5 ECAL cell window, containing γ^{dir} candidate in the center.

$**$ scalar sum of P_t in the 5x5 ECAL cell window in the region out of a smaller 3x3 window, containing γ.

shall apply the following cuts on the observable physical variables one after another according to the list presented below. The influence of these cuts on the S/B ratio is demonstrated in the following Tables 2–8. The numbers in the left-hand column ("Cut"≡"Selection") of Table 2, that corresponds to $P_t{}^{\gamma} \geq 100\ GeV/c$, coincide with the numbers of cuts listed below, where for abbreviation reasons we shall denote the direct photon by "γ" as well as its candidate.

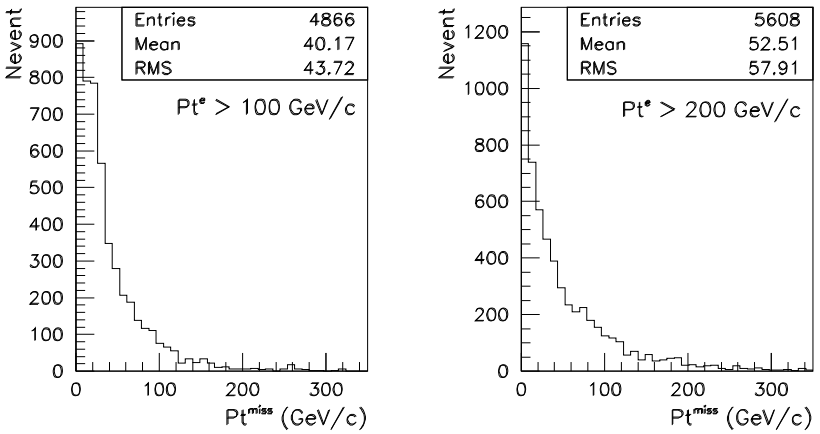

Fig. 7: Distribution of events over $P_t{}^{miss}$ in events with energetic $e^{\pm}$'s – direct photon candidates for the cases $P_t{}^{e} \geq 100\ GeV/c$ and $P_t{}^{e} \geq 200\ GeV/c$ (here are used events satisfying cuts 1–3 of Table 1).

From the first line of Table 2 we see that without imposing any cut, the number of the background events exceeds the number of the signal events, caused by (1a) and (1b) processes, by 5 orders. The relative isolation cut 2 ($\epsilon^{\gamma} \leq 15\%$) makes the S/B ratio equal to 0.28. The cut 3 ($P_t{}^{\gamma} \geq \hat{p}_{\perp}^{\,min}$) improves the S/B ratio to 0.68. The relative isolation cut 5 and then the absolute isolation cut 6 make the S/B ratio to be equal to 1.50 and 1.93,

respectively. The requirement of only one jet presence in the event (point 9) results in the value $S/B = 5.96$. The ratio S/B is increased by the cut $\Delta\phi < 15^\circ$ up to the value 6.54 (point 10) and at the same time the number of signal events is decreased only by 5%. This is in agreement with the phenomenon of the concentration of events in the small $\Delta\phi$ angle at large ${P_t}^\gamma$ values already mentioned in paper [2].

We have used the P_{tCUT}^{miss} cut in paper [1] to reduce value of ${P_t}^{Jet}$ uncertainty due to possible presence of neutrino contribution to a jet. Here it is applied against the processes based (at the parton level) on the $q\,g \to q' + W^\pm$ and $q\,\bar{q}' \to g + W^\pm$ subprocesses with the subsequent decay $W^\pm \to e^\pm\nu$ and having for this reason a substantial ${P_t}^{miss}$ value. The distributions over ${P_t}^{miss}$ for two ${P_t}^e$ values are presented above. In the last column ($e^\pm$) of Table 2 it is shown how the P_{tCUT}^{miss} cut effects the number of these events (point 11).

The reduction of P_{tCUT}^{clust} value to 10 GeV/c (point 14) results in significant improvement of S/B ratio up to 17.64. Further reduction of P_{tCUT}^{out} value to 10 GeV/c (point 17) improves S/B to 22.67. The jet isolation requirement $\epsilon^{jet} < 2\%$ (point 19), finally, gives $S/B = 31.05$.

Table 2: Values of significance and efficiencies for $\hat{p}_\perp^{\,min}$=100 GeV/c

Cut	S	B *	$Eff_S(\%)$	$Eff_B(\%)$	S/B	$e^\pm$
0	19420	5356.E+6			0.00	3.9E+6
1	19359	1151425	100.00 ± 0.00	100.000 ± 0.000	0.02	47061
2	18236	65839	94.20 ± 0.97	5.718 ± 0.023	0.28	8809
3	15197	22437	78.50 ± 0.85	1.949 ± 0.013	0.68	2507
4	15174	19005	78.38 ± 0.85	1.651 ± 0.012	0.80	2486
5	14140	9433	73.04 ± 0.81	0.819 ± 0.008	1.50	2210
6	8892	4618	45.93 ± 0.59	0.401 ± 0.006	1.93	1331
7	8572	3748	44.28 ± 0.57	0.326± 0.005	2.29	1174
8	7663	2488	39.58 ± 0.53	0.216± 0.004	3.08	921
9	4844	813	25.02 ± 0.40	0.071± 0.002	5.96	505
10	4634	709	23.94 ± 0.39	0.062 ± 0.002	6.54	406
11	4244	650	21.92 ± 0.37	0.056 ± 0.002	6.53	87
12	3261	345	16.84 ± 0.32	0.030 ± 0.002	9.45	53
13	2558	194	13.21 ± 0.28	0.017 ± 0.001	13.19	41
14	1605	91	8.29 ± 0.22	0.008 ± 0.001	17.64	26
15	1568	86	8.10 ± 0.21	0.007 ± 0.001	18.23	26
16	1477	77	7.63 ± 0.21	0.007 ± 0.001	19.18	25
17	1179	52	6.09 ± 0.18	0.005 ± 0.001	22.67	22
18	1125	46	5.81 ± 0.18	0.004 ± 0.001	24.46	21
19	683	22	3.53 ± 0.14	0.002 ± 0.000	31.05	13

$*$ The background is considered here with no account of contribution from the " $e^\pm$ events"

The summary of Table 2 is presented in the middle section ($\hat{p}_\perp^{\,min} = 100\ GeV/c$) of Table 3 where in the second column ("Cuts") line "Preselected" corresponds to the 1-st cut of the Table 2 presented above. Line "After cuts" corresponds to line 17 and line "+jet isolation" — to the complementary line 19.

In Table 3 the numbers in column "$\gamma - direct$" correspond, respectively, to the numbers of the signal events in column S of Table 2 in lines 1, 17 and 19 while the numbers in the 4-th column "$\gamma - brem$" correspond to the number of events with the photons radiated from quarks participating in the hard interactions (their P_t^{clust} and P_t^{out} distributions were presented in the central columns of Figs. 1–6 of Section 2). The columns from 5-th to 8-th of Table 3 illustrate the numbers of the events with the photons "$\gamma - mes$", originated from π^0-, $\eta-$, $\omega-$, K_S^0- meson decays (their distributions were shown in the right-hand columns of the same Figs. 1–6. The total number of the background events without an account of events with electrons (see last column), i.e. a sum over columns 4–8 , for the same line of Table 3 is presented, correspondingly, in the column B of Table 2.

Table 3: Number of signal and background events remained after cuts **(I)**

$\hat{p}_\perp^{min}$ (GeV/c)	Cuts	γ direct	γ brem	photons from the mesons				$e^\pm$
				π^0	η	ω	K_S^0	
40	Preselected	7795	12951	104919	41845	10984	15058	4204
	After cuts	516	48	41	10	0	5	0
	+ jet isol.	122	7	5	1	0	1	0
100	Preselected	19359	90022	658981	247644	69210	85568	47061
	After cuts	1179	34	13	4	1	0	22
	+ jet isol.	683	15	5	2	0	0	13
200	Preselected	32629	207370	780190	288772	82477	98015	89714
	After cuts	1074	18	2	4	0	0	10
	+ jet isol.	916	16	1	4	0	0	8

Table 4: Efficiencies and significance values in events without jet isolation cut **(I)**

$\hat{p}_\perp^{min}$ (GeV/c)	S	B	$Eff_S(\%)$	$Eff_B(\%)$	S/B	$S/\sqrt{B}$
40	516	104	6.62 ± 0.30	0.056 ± 0.005	5.0	50.6
100	1179	52	6.09 ± 0.18	0.005 ± 0.001	22.7	163.5
200	1074	24	3.29 ± 0.10	0.002 ± 0.000	44.8	219.2

Table 5: Efficiencies and significance values in events with jet isolation cut **(I)**

$\hat{p}_\perp^{min}$ (GeV/c)	S	B	$Eff_S(\%)$	$Eff_B(\%)$	S/B	$S/\sqrt{B}$
40	122	14	1.57 ± 0.14	0.008 ± 0.002	8.7	32.6
100	683	22	3.53 ± 0.14	0.002 ± 0.000	31.1	145.6
200	916	21	2.81 ± 0.09	0.001 ± 0.000	43.6	199.9

The other lines of Table 3 for cases $\hat{p}_\perp^{min} = 40$ and $200\ GeV/c$ have the meaning analogous to those described above for $\hat{p}_\perp^{min} = 100\ GeV/c$.

The last column of Table 3 shows the number of the events with electrons which with non-zero probability can be detected as direct photon. The following columns of Table 2 define efficiencies $Eff_{S(B)}$ (and their errors) as a ratio of the number of signal (background) events that passed under some cut (1–19) to the number of the preselected events (1-st cut of this table). The last column of Table 2 contains the values of significances (without account

of events with electrons). The numbers in Tables 4 and 5 accumulate in compact form the information of Table 3. So, for the middle line ($\hat{p}_\perp^{min} = 100\ GeV/c$ case) columns S and B contain the numbers of the signal and background events taken at the level of line 17 (for Table 4) and line 19 for Table 2). The column $Eff_{S(B)}$ includes the values of efficiencies [4] and their errors.

Table 6: Signal vs. background **(II)**

$\hat{p}_\perp^{min}$ (GeV/c)	Cuts	γ direct	γ brem	photons from the mesons				$e^\pm$
				π^0	η	ω	K_S^0	
40	Preselected	7795	12951	104919	41845	10984	15058	4204
	After cuts	464	43	15	0	0	0	0
	+ jet isol.	109	7	2	0	0	0	0
100	Preselected	19359	90022	658981	247644	69210	85568	47061
	After cuts	1061	31	9	0	0	0	3
	+ jet isol.	615	14	4	0	0	0	2
200	Preselected	32629	207370	780190	288772	82477	98015	89714
	After cuts	967	16	2	0	0	0	2
	+ jet isol.	825	14	1	0	0	0	1

Table 7: Values of efficiencies and significance **(II)**

$\hat{p}_\perp^{min}(GeV/c)$	S	B	$Eff_S(\%)$	$Eff_B(\%)$	S/B	$S/\sqrt{B}$
40	464	58	5.95 ± 0.28	0.031 ± 0.004	8.0	60.9
100	1061	43	5.48 ± 0.17	0.004 ± 0.001	24.7	161.8
200	967	20	2.96 ± 0.10	0.002 ± 0.000	48.4	216.2

Table 8: Values of efficiencies and significance with jet isolation cut **(II)**

$\hat{p}_\perp^{min}(GeV/c)$	S	B	$Eff_S(\%)$	$Eff_B(\%)$	S/B	$S/\sqrt{B}$
40	109	9	1.40 ± 0.13	0.005 ± 0.002	12.1	36.3
100	615	20	3.18 ± 0.13	0.003 ± 0.000	30.8	137.5
200	825	16	2.53 ± 0.09	0.002 ± 0.000	51.6	206.3

From Table 4 it is seen that ratio S/B grows while the ${P_t}^\gamma$ value growing from 5.0 at ${P_t}^\gamma \geq 40\ GeV/c$ to 44.8 at ${P_t}^\gamma \geq 200\ GeV/c$. The jet isolation requirement (Table 5) sufficiently improves the situation at low P_t. In that case S/B changes up to 8.7 at ${P_t}^\gamma \geq 40\ GeV/c$ (and up to 31.1 at ${P_t}^\gamma \geq 100\ GeV/c$). Here it is necessary to remind about the conclusion on the tendency of the selected events to contain an isolated jet: their number grows while the ${P_t}^\gamma$ value increasing. Practically all jets with ${P_t}^{Jet} \geq 200\ GeV/c$ are isolated (compare two last lines of Table 3) [5].

Up to now we have not used the rejection factors, that were found basing on the detector capability to discriminate the background. Let us discuss how the values in Tables

[4] taken as a ratio of the number of signal S (background B) events, that passed under cut 17 or 19, to the number of the preselected events in the point 1 of Table 2.

[5] see also Fig. 10 for ${P_t}^\gamma \geq 300\ GeV/c$ from [1]

2–5 can be changed by taking into account the real behavior of processes in the detectors.

We have performed a detailed study (based on CMSIM GEANT simulation using 5000 generated decays of each source meson from Table 3) of difference between ECAL profiles of photon showers from mesons and those from direct photons for ${P_t}^{\gamma} = 40 \div 100\, GeV/c$. It has shown that the suppression factor of η-, ω-, K^0_S-mesons larger than 0.90 can be achieved with a selection efficiency of single photons taken to be 90%. As for the photons from π^0 decays, the analogous estimations of the rejection efficiencies were done for the Endcap

In Tables 3 and 6 we have not presented separately the background due to γ/jet misidentification because as it was shown in [9], γ and jet can be discriminated with a high precision and, secondly, as it was mentioned in Section 2 of this paper (see also Section 3.2 of [1]), we have defined the photon (or the candidate to be registered as the direct photon) as the signal in the 3x3 ECAL crystal cell window satisfying cut conditions (17) – (22) of Section 3.2 of [1]. These cuts effectively discriminate the photons from jets.

In Section 2 it has been shown that even with moderate cuts on P_{tCUT}^{clust} and P_{tCUT}^{out} values the major part of the background events can be suppressed. A wide variation of these two cuts and their influence on the number of events (for $L_{int} = 3\, fb^{-1}$), and the corresponding values of the signal to background ratio S/B, mean values of vector disbalance ${P_t}^{\gamma+Jet}$, the mean and the standard deviation values for $({P_t}^{\gamma} - {P_t}^{Jet})/{P_t}^{\gamma}$ variable are presented in Tables 11 – 25 of Appendix. These tables are built after selections (1) – (11) of Table 1 in the beginning of Section 3. The jet in our 1-jet events was found by LUCELL jetfinder for the whole η region ($|\eta^{jet}| < 5.0$).

Tables 11 – 15 correspond to the simulation with $\hat{p}_{\perp}^{min} = 40\ GeV/c$, Tables 16 – 20 — to $\hat{p}_{\perp}^{min} = 100\ GeV/c$ and Tables 21 – 25 — to $\hat{p}_{\perp}^{min} = 200\ GeV/c$. The rows and columns of Tables 11 – 25 illustrate the influence of P_{tCUT}^{clust} and P_{tCUT}^{out} cut values on the quantities mentioned above, respectively.

All numbers in Tables 11 – 25 are received with account of the realistic efficiencies of γ^{mes} rejection and electron misidentification as a direct photon.

From Tables 12, 17, 22 and 27, 32, 37 we observe, first of all, noticeable reduction of the background while moving along the diagonal from the right-hand bottom corner to the left-hand upper one, i.e. with reinforcing P_{tCUT}^{clust} and P_{tCUT}^{out}. So, we see that for $\hat{p}_{\perp}^{min} = 40\ GeV/c$ the ratio S/B changes in the cells along the diagonal from 3.2, if any limits on these two variables are absent, to 6.5 for $P_{tCUT}^{clust} = 10\ GeV/c$ and $P_{tCUT}^{out} = 10\ GeV/c$. Analogously, for $\hat{p}_{\perp}^{min} = 200\ GeV/c$ the ratio S/B changes from 12.5 to 48.4 with the same variation of P_{tCUT}^{clust} and P_{tCUT}^{out}.

The second observation. The restriction of ${P_t}^{clust}$ and ${P_t}^{out}$ improves the calibration accuracy. Table 14 shows that the mean value of fraction $F \equiv ({P_t}^{\gamma} - {P_t}^{Jet})/{P_t}^{\gamma}$ variable decreases from 0.033 (the bottom right-hand corner) to 0.008 for $P_{tCUT}^{clust} = 10\ GeV/c$ and $P_{tCUT}^{out} = 10\ GeV/c$. Simultaneously (see Tables 15, 20 and 25 that include the standard deviation values), by this restriction one decreases noticeably (about by twice) the width of the gaussian $\sigma(F)$.

The explanation is simple. The disbalance equation (29) from [1] contains 2 terms in the right-hand side: $(1 - cos\Delta\phi)$ and $P_t(O{+}\eta > 5)/{P_t}^{\gamma}$. The first one is negligibly small and tends to decrease more with the growth of ${P_t}^{\gamma}$ (see Tables in Appendices of [3]). So, according to equation (29) of [1], the main source of the disbalance value is $P_t(O{+}\eta > 5)/{P_t}^{\gamma}$

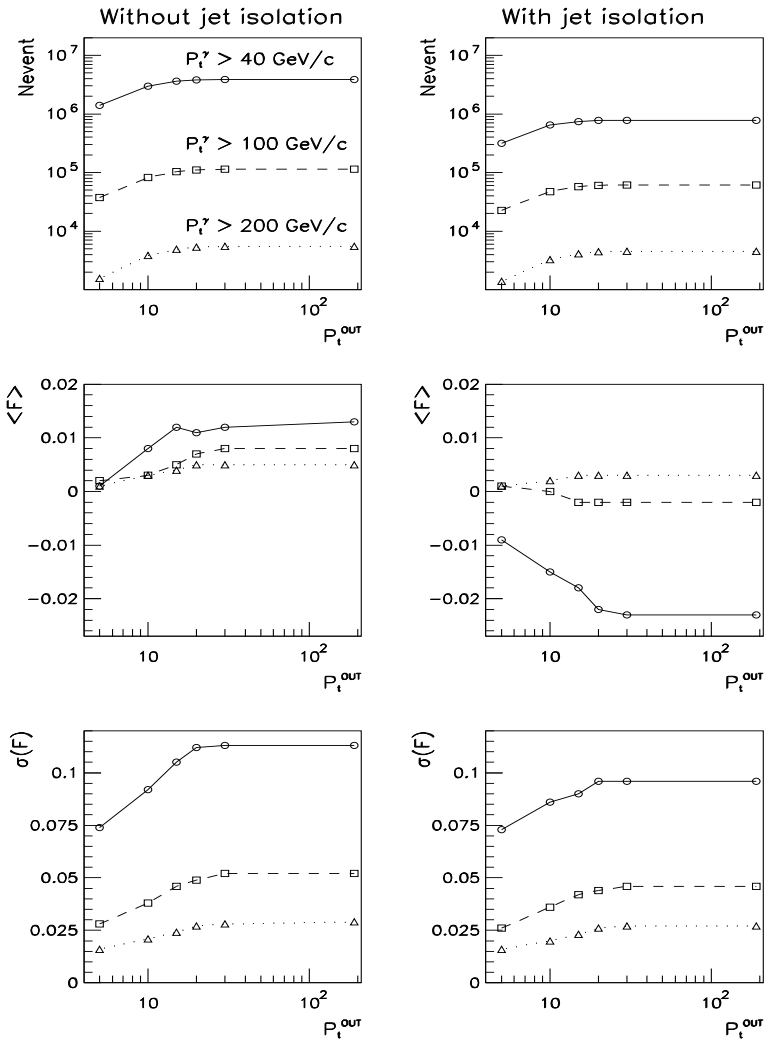

Fig. 8: The distributions of the number of events for $L_{int} = 3\ fb^{-1}$, the mean value of $(P_t{}^\gamma - P_t{}^{Jet})/P_t{}^\gamma$ ($\equiv \langle F \rangle$) and its standard deviation $\sigma(F)$ for the cases of nonisolated (left-hand column) and isolated (right-hand column) jet and for three $P_t{}^\gamma$ intervals as functions of $P_t{}^{out}$ value (in GeV/c). $P_{t\,CUT}^{clust} = 10\ GeV/c$.

[6, 8] and Barrel [6, 7] ECAL regions. They are of the order of 0.20 – 0.70 for Barrel and 0.51 – 0.75 for Endcap, depending on $P_t{}^\gamma$ and a bit on η^γ, for the same single photon selection efficiency 90%. Following [5], for our estimation needs we accept the electron track finding efficiency to be, on the average, equal to 85% for $P_t{}^e \geq 40\ GeV/c$, neglecting its η dependence. Then assuming the efficiencies, described above, we have recalculated the numbers in Tables 3–5. They are presented in new Tables 6–8 in the analogy with Tables 3–5 (the background (B) in Tables 6–8 differs from one in Tables 3–5 by including the events with electron candidates with the corresponding efficiencies). Comparing new tables with Tables 3–5 we observe the $50 - 60\%$ growth of S/B ratio for $P_t{}^\gamma \geq 40\ GeV/c$ and about the 10% growth for $P_t{}^\gamma \geq 100\ GeV/c$.

term. While decreasing P_t activity out of the jet this term is also decreased and, thus, the calibration accuracy is increased.

The behavior of the number of events for $L_{int} = 3\,fb^{-1}$, the mean and standard deviation values of the $(P_t{}^{\gamma} - P_t{}^{Jet})/P_t{}^{\gamma}$ variable are also displayed in Fig. 8 for isolated and nonisolated jets.

Thus, we can conclude that application of the two criteria introduced in Section 3.2 from [1], i.e. the cuts on the $P_t{}^{clust}$ and $P_t{}^{out}$ values, results in two important consequences: significant background reduction and essential improvement of the calibration accuracy.

In Tables 13, 18, 23 the changes of vector disbalance $P_t{}^{\gamma+Jet}$ with variations of the cuts on the $P_t{}^{clust}$ and $P_t{}^{out}$ values are presented. The effect is also evident. The only obvious notice: the value of $P_t{}^{\gamma+Jet}$ in the upper left-hand corner of these Tables (i.e., when a P_t activity out of a the jet region is almost suppressed), becomes approximately equal to the value of $P_t{}^{\eta>5}$ component (see line "$P_t{}^{\eta>5}$" in Appendices of [3]).

The numbers of events for different P_{tCUT}^{clust} and P_{tCUT}^{out} values are written in the cells of Tables 11, 16 and 21. One can see that even with such strict P_{tCUT}^{clust} and P_{tCUT}^{out} values as, i.g. $10\ GeV/c$ for both, we would have a sufficient number of events (3 million, about 80 thousand and 4 thousand for $P_t{}^{\gamma} \geq 40\ GeV/c$, $P_t{}^{\gamma} \geq 100\ GeV/c$ and $P_t{}^{\gamma} \geq 200\ GeV/c$, correspondingly) with low background contamination ($S/B = 6.5,\ 24.7,\ 48.4$) as well as good accuracy of the hadron calorimeter calibration during one month of continuous LHC running (i.e. $L_{int} = 3\ fb^{-1}$) [6].

In addition, we also present Tables 26-40 for the case of the isolated jet by the complete analogy with Tables 11–25.

4. STUDY OF P_t BALANCE DEPENDENCE ON PARTON k_T.

This Section is dedicated to the study of possible influence of the intrinsic parton transverse momentum on P_t balance of the "$\gamma + Jet$" system. For this aim we consider two different

Table 9: Effect of k_T on $P_t{}^{\gamma}$ - $P_t{}^{Jet}$ balance with $\hat{p}_{\perp}^{min}$=40 GeV/c. $F = (P_t{}^{\gamma} - P_t{}^{Jet})/P_t{}^{\gamma}$

$\langle k_T \rangle$	ISR is OFF				ISR is ON			
(GeV/c)	$\langle P_t 56 \rangle$	$\langle P_t{}^{5+6} \rangle$	$\langle F \rangle$	$\sigma(F)$	$\langle P_t 56 \rangle$	$\langle P_t{}^{5+6} \rangle$	$\langle F \rangle$	$\sigma(F)$
0.0	0.0	0.0	-0.002	0.029	8.8	6.9	0.007	0.065
1.0	1.8	1.3	-0.001	0.036	9.1	7.0	0.009	0.069
2.5	4.5	3.2	0.001	0.054	9.6	7.4	0.010	0.074
5.0	8.7	6.1	0.014	0.089	10.4	7.2	0.015	0.088
7.0	11.2	7.7	0.020	0.107	11.0	8.2	0.022	0.101

ranges of $P_t{}^{\gamma}$ (or $\hat{p}_{\perp}^{min}$): $\hat{p}_{\perp}^{min} \geq 40\ GeV/c$ and $\hat{p}_{\perp}^{min} \geq 200\ GeV/c$. For these two $\hat{p}_{\perp}^{min}$ values Tables 9 and 10 demonstrate the average values of $P_t 56$ and $P_t{}^{5+6}$ quantities, defined by (3) of [1], for two different cases: without including initial state radiation ("ISR is OFF") and with its account ("ISR is ON"), and various values of parton $\langle k_T \rangle$: from its absence

[6] Nevertheless, only full GEANT simulation would allow to come to a final conclusion.

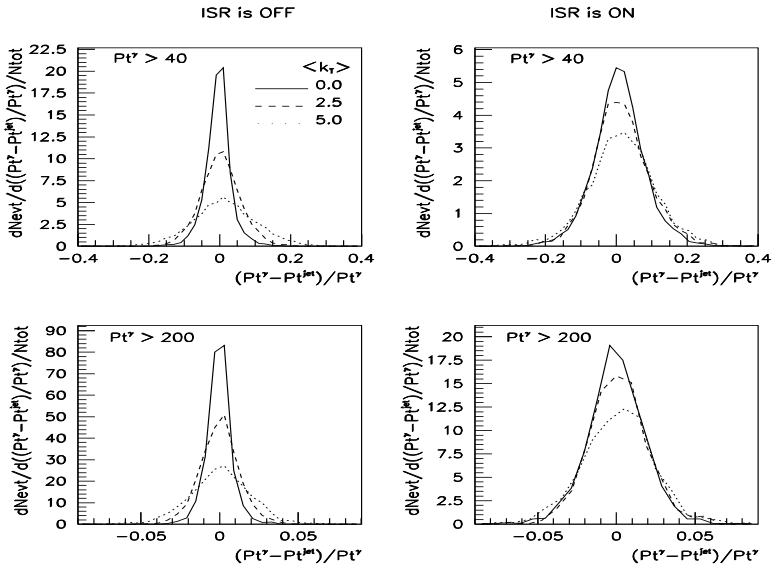

Fig. 9: $(P_t{}^{\gamma}-P_t{}^{Jet})/P_t{}^{\gamma}$ as a function of primordial k_T value for cases of switched on and switched off initial radiation and for $\hat{p}_\perp^{\,min} = 40$ and $\hat{p}_\perp^{\,min} = 200\ \ GeV/c$.

Table 10: Effect of k_T on $P_t{}^{\gamma}$ -$P_t{}^{Jet}$ balance with $\hat{p}_\perp^{\,min}$=200 GeV/c. $F = (P_t{}^{\gamma}-P_t{}^{Jet})/P_t{}^{\gamma}$

$\langle k_T\rangle$	ISR is OFF				ISR is ON			
(GeV/c)	$\langle P_t 56\rangle$	$\langle P_t{}^{5+6}\rangle$	$\langle F\rangle$	$\sigma(F)$	$\langle P_t 56\rangle$	$\langle P_t{}^{5+6}\rangle$	$\langle F\rangle$	$\sigma(F)$
0.0	0.0	0.0	0.000	0.010	11.1	8.4	-0.001	0.027
1.0	1.8	1.3	0.000	0.013	11.2	8.6	0.000	0.028
2.5	4.5	3.1	0.000	0.019	11.8	8.8	0.001	0.028
5.0	8.7	6.1	0.001	0.022	12.7	9.3	0.001	0.031
7.0	11.2	7.8	0.001	0.029	13.9	10.4	0.002	0.034

$*$ All numbers in the tables above are given in GeV/c units.

($\langle k_T\rangle = 0$) up to $\langle k_T\rangle = 7\ GeV/c$. The numbers in Tables 9 and 10 (obtained from the events set chosen by the following cuts: $\Delta\phi < 15^\circ$, $P_{tCUT}^{out} = 5\ GeV/c$ and $P_{tCUT}^{clust} = 10\ GeV/c$) have shown that the values of $\langle P_t 56\rangle$ and $\langle P_t 56\rangle$ grow rapidly with $\langle k_T\rangle$ increasing if ISR is absent, in fact, with the values of $\langle k_T\rangle$. The picture changes when ISR is included. In this case the disbalance values become large already in the case of $\langle k_T\rangle = 0$: $\langle P_t 56\rangle = 8.8\ GeV/c$ at $\hat{p}_\perp^{\,min} = 40\ GeV/c$ and $\langle P_t{}^{5+6}\rangle = 11.1\ GeV/c$ at $\hat{p}_\perp^{\,min} = 200\ GeV/c$. The values of $\langle P_t 56\rangle$ and $\langle P_t{}^{5+6}\rangle$ grow very slowly from their initial values at $\langle k_T\rangle = 0$ by $2-3\ GeV/c$ showing their practical independence on $\langle k_T\rangle$ in the range of its reasonable value $\langle k_T\rangle \leq 1\ GeV/c$.

The size of relative disbalance $F = (P_t{}^{\gamma}-P_t{}^{Jet})/P_t{}^{\gamma}$ variation with k_T is also shown in Tables 9 and 10 and in plots of Fig. 9. One can see that for reasonable values $\langle k_T\rangle \leq 1\ GeV/c$ it is quite small.

5. ACKNOWLEDGMENTS

We are greatly thankful to D. Denegri for having offered this theme to study, fruitful discussions and permanent support and encouragement. It is a pleasure for us to express our recognition for helpful discussions to P. Aurenche, M. Dittmar, M.L. Mangano, H. Rohringer, S. Taprogge, M. Fontannaz, J.Ph. Guillet, E. Pilon and J. Womersley.

References

[1] D.V. Bandourin, V.F. Konoplyanikov, N.B. Skachkov. "Jet energy scale setting with "$\gamma + Jet$" events at LHC energies. Generalities, selection rules", JINR Preprint E2-2000-251, JINR, Dubna.

[2] D.V. Bandourin, V.F. Konoplyanikov, N.B. Skachkov. "Jet energy scale setting with "$\gamma + Jet$" events at LHC energies. Event rates, P_t structure of jet", JINR Preprint E2-2000-252, JINR, Dubna.

[3] D.V. Bandourin, V.F. Konoplyanikov, N.B. Skachkov. "Jet energy scale setting with "$\gamma + Jet$" events at LHC energies. Minijets and cluster suppression and ${P_t}^{\gamma} - {P_t}^{Jet}$ disbalance", JINR Preprint E2-2000-253, JINR, Dubna.

[4] D.V. Bandourin, V.F. Konoplyanikov, N.B. Skachkov. "Jet energy scale setting with "$\gamma + Jet$" events at LHC energies. Selection of events with a clean "$\gamma + Jet$" topology and ${P_t}^{\gamma} - {P_t}^{Jet}$ disbalance", JINR Preprint E2-2000-254, JINR, Dubna.

[5] CMS Tracker Project, Technical Design Report, CERN/LHCC 98–6, CMS TDR 5, p. 488.

[6] CMS Electromagnetic Calorimeter Project, Technical Design Report, CERN/LHCC 97–33, CMS TDR 4, p. 326.

[7] S. Shevchenko et al., CMS Note 1997/050, "Neutral pion rejection in the CMS $PbWO_4$ crystal calorimeter using a neural network"

[8] A. Kyriakis, D. Loukas, J. Mousa, D. Barney, CMS Note 1998/088, "Artificial neural net approach to $\gamma - \pi^0$ discrimination using CMS Endcap Preshower".

[9] F. Gianotti, I. Vichou, ATLAS Note PHYS-No-78, 1996, γ/jet separation with the ATLAS detector".

APPENDIX

$$\hat{p}_{\perp}^{\,min} = 40\ GeV/c.$$

Table 11: Number of events per $L_{int} = 3\ fb^{-1}$

$P_{t\ cut}^{\ clust}$ (GeV/c)	$P_{t\ cut}^{\ out}\ (GeV/c)$					
	5	10	15	20	30	1000
5	523000	885000	921000	921000	921000	921000
10	1399000	2994000	3642000	3803000	3838000	3841000
15	1598000	3809000	5059000	5576000	5745000	5748000
20	1678000	4112000	5638000	6408000	6818000	6841000
30	1739000	4328000	6082000	7101000	7873000	8101000

Table 12: S/B

$P_{t\ cut}^{\ clust}$ (GeV/c)	$P_{t\ cut}^{\ out}\ (GeV/c)$					
	5	10	15	20	30	1000
5	11.6± 4.2	9.2± 2.4	8.8± 2.2	8.8± 2.2	8.8± 2.2	8.8± 2.2
10	8.0± 1.5	6.5± 0.8	5.7± 0.6	5.6± 0.6	5.7± 0.6	5.7± 0.6
15	6.3± 1.1	5.4± 0.6	4.7± 0.4	4.6± 0.4	4.4± 0.4	4.4± 0.4
20	6.1± 1.0	4.8± 0.5	4.1± 0.3	3.9± 0.3	3.8± 0.3	3.8± 0.3
30	5.7± 0.9	4.2± 0.4	3.6± 0.3	3.5± 0.2	3.2± 0.2	3.2± 0.2

Table 13: $\langle {P_t}^{\gamma+Jet} \rangle\ (GeV/c)$

$P_{t\ cut}^{\ clust}$ (GeV/c)	$P_{t\ cut}^{\ out}\ (GeV/c)$					
	5	10	15	20	30	1000
5	3.8	4.5	4.7	4.7	4.7	4.7
10	4.2	5.4	6.2	6.6	6.7	6.7
15	4.2	5.7	7.0	7.7	8.1	8.1
20	4.3	5.8	7.2	8.3	9.1	9.1
30	4.3	5.9	7.5	8.7	10.0	10.8

Table 14: $\langle F \rangle,\ F = ({P_t}^{\gamma} - {P_t}^{Jet})/{P_t}^{\gamma}$

$P_{t\ cut}^{\ clust}$ (GeV/c)	$P_{t\ cut}^{\ out}\ (GeV/c)$					
	5	10	15	20	30	1000
5	0.005	0.006	0.007	0.007	0.007	0.007
10	0.001	0.008	0.012	0.011	0.012	0.013
15	0.004	0.010	0.017	0.019	0.022	0.022
20	0.005	0.011	0.021	0.024	0.029	0.029
30	0.004	0.011	0.022	0.026	0.032	0.033

Table 15: $\sigma(F),\ F = ({P_t}^{\gamma} - {P_t}^{Jet})/{P_t}^{\gamma}$

$P_{t\ cut}^{\ clust}$ (GeV/c)	$P_{t\ cut}^{\ out}\ (GeV/c)$					
	5	10	15	20	30	1000
5	0.069	0.081	0.085	0.085	0.085	0.085
10	0.074	0.092	0.105	0.112	0.113	0.113
15	0.076	0.098	0.118	0.134	0.140	0.141
20	0.076	0.100	0.123	0.144	0.158	0.159
30	0.077	0.102	0.127	0.152	0.173	0.177

$$\hat{p}_{\perp}^{\,min} = 100\ GeV/c.$$

Table 16: Number of events per $L_{int} = 3\ fb^{-1}$

$P_{t\,cut}^{\,clust}$ (GeV/c)	$P_{t\,cut}^{\,out}\ (GeV/c)$					
	5	10	15	20	30	1000
5	14100	24600	27000	27200	27300	27400
10	37700	82400	103800	110600	113500	113600
15	44900	106300	146800	168500	183300	184200
20	47100	114600	166600	200900	234300	241400
30	48900	121200	180600	227900	293900	327200

Table 17: S/B

$P_{t\,cut}^{\,clust}$ (GeV/c)	$P_{t\,cut}^{\,out}\ (GeV/c)$					
	5	10	15	20	30	1000
5	59.0±38.2	44.3±19.2	40.7±16.2	41.0±16.4	41.0±16.4	41.0±16.4
10	25.0± 6.5	24.7± 4.6	21.4± 3.3	20.5± 3.0	19.5± 2.8	19.8± 2.8
15	23.9± 6.0	19.3± 2.9	16.1± 1.9	15.2± 1.6	14.1± 1.4	14.1± 1.4
20	19.6± 4.4	15.9± 2.1	12.8± 1.3	12.0± 1.1	10.1± 0.8	9.9± 0.8
30	18.6± 4.0	13.6± 1.7	11.0± 1.0	9.2± 0.7	7.4± 0.5	6.8± 0.4

Table 18: $\langle {P_t}^{\gamma+Jet} \rangle\ (GeV/c)$

$P_{t\,cut}^{\,clust}$ (GeV/c)	$P_{t\,cut}^{\,out}\ (GeV/c)$					
	5	10	15	20	30	1000
5	3.7	4.7	5.2	5.3	5.4	5.5
10	4.0	5.5	6.6	7.2	7.5	7.6
15	4.2	5.9	7.5	8.6	9.7	9.8
20	4.3	6.1	7.9	9.4	11.3	11.9
30	4.4	6.1	8.1	10.0	13.0	15.5

Table 19: $\langle F \rangle,\ F = ({P_t}^{\gamma} - {P_t}^{Jet})/{P_t}^{\gamma}$

$P_{t\,cut}^{\,clust}$ (GeV/c)	$P_{t\,cut}^{\,out}\ (GeV/c)$					
	5	10	15	20	30	1000
5	0.002	0.001	0.003	0.004	0.004	0.005
10	0.002	0.003	0.005	0.007	0.008	0.008
15	0.001	0.003	0.006	0.009	0.013	0.013
20	0.002	0.003	0.006	0.011	0.016	0.019
30	0.002	0.003	0.005	0.011	0.019	0.027

Table 20: $\sigma(F),\ F = ({P_t}^{\gamma} - {P_t}^{Jet})/{P_t}^{\gamma}$

$P_{t\,cut}^{\,clust}$ (GeV/c)	$P_{t\,cut}^{\,out}\ (GeV/c)$					
	5	10	15	20	30	1000
5	0.028	0.035	0.038	0.038	0.039	0.039
10	0.028	0.038	0.046	0.049	0.052	0.052
15	0.029	0.041	0.051	0.057	0.065	0.066
20	0.030	0.042	0.053	0.062	0.075	0.080
30	0.030	0.043	0.055	0.067	0.087	0.101

$$\hat{p}_{\perp}^{\,min} = 200\ GeV/c.$$

Table 21: Number of events per $L_{int} = 3\ fb^{-1}$

$P_{t\ cut}^{\ clust}$ (GeV/c)	$P_{t\ cut}^{\ out}\ (GeV/c)$					
	5	10	15	20	30	1000
5	570	1090	1180	1210	1220	1230
10	1550	3830	4900	5360	5470	5490
15	1960	5060	7360	8710	9500	9630
20	2110	5590	8480	10550	12410	12990
30	2170	5880	9210	11830	15510	18270

Table 22: S/B

$P_{t\ cut}^{\ clust}$ (GeV/c)	$P_{t\ cut}^{\ out}\ (GeV/c)$					
	5	10	15	20	30	1000
5	109 ± 109	173 ± 154	115 ± 82	118 ± 84	118 ± 84	118 ± 84
10	50.7±16.0	48.4±13.3	44.1±10.2	37.4± 7.6	38.2± 7.8	38.2± 7.8
15	38.5±13.2	44.1±10.0	35.9± 6.2	27.9± 4.0	25.7± 3.4	25.4± 3.3
20	29.3± 8.6	36.4± 7.2	26.5± 3.7	22.0± 2.6	18.8± 1.9	17.2± 1.7
30	28.6± 8.2	28.2± 4.9	20.6± 2.5	17.4± 1.8	14.5± 1.2	12.5± 0.9

Table 23: $\langle {P_t}^{\gamma+Jet} \rangle\ (GeV/c)$

$P_{t\ cut}^{\ clust}$ (GeV/c)	$P_{t\ cut}^{\ out}\ (GeV/c)$					
	5	10	15	20	30	1000
5	4.0	5.0	5.4	5.6	5.7	6.1
10	4.5	6.0	7.0	7.8	8.1	8.2
15	4.6	6.2	7.9	9.2	10.4	10.7
20	4.7	6.3	8.2	9.9	11.9	13.0
30	4.7	6.4	8.5	10.4	13.7	17.5

Table 24: $\langle F \rangle,\ F = ({P_t}^{\gamma} - {P_t}^{Jet})/{P_t}^{\gamma}$

$P_{t\ cut}^{\ clust}$ (GeV/c)	$P_{t\ cut}^{\ out}\ (GeV/c)$					
	5	10	15	20	30	1000
5	0.003	0.003	0.003	0.004	0.004	0.005
10	0.001	0.003	0.004	0.005	0.005	0.005
15	0.001	0.003	0.006	0.007	0.008	0.008
20	0.001	0.003	0.005	0.007	0.008	0.010
30	0.001	0.003	0.005	0.007	0.009	0.014

Table 25: $\sigma(F),\ F = ({P_t}^{\gamma} - {P_t}^{Jet})/{P_t}^{\gamma}$

$P_{t\ cut}^{\ clust}$ (GeV/c)	$P_{t\ cut}^{\ out}\ (GeV/c)$					
	5	10	15	20	30	1000
5	0.015	0.018	0.020	0.021	0.023	0.026
10	0.016	0.021	0.024	0.027	0.028	0.029
15	0.016	0.021	0.027	0.031	0.035	0.037
20	0.016	0.022	0.028	0.033	0.040	0.044
30	0.016	0.022	0.029	0.035	0.046	0.057

$$\hat{p}_{\perp}^{\,min} = 40\ GeV/c, \quad \epsilon^{jet} < 2\%.$$

Table 26: Number of events per $L_{int} = 3\ fb^{-1}$

$P_{t\ cut}^{\ clust}$ (GeV/c)	$P_{t\ cut}^{\ out}\ (GeV/c)$					
	5	10	15	20	30	1000
5	165000	278000	284000	284000	284000	284000
10	317000	652000	739000	772000	778000	778000
15	332000	737000	890000	970000	994000	994000
20	355000	779000	958000	1074000	1124000	1124000
30	361000	805000	1000000	1146000	1266000	1308000

Table 27: S/B

$P_{t\ cut}^{\ clust}$ (GeV/c)	$P_{t\ cut}^{\ out}\ (GeV/c)$					
	5	10	15	20	30	1000
5	8.6± 5.0	12.6± 6.5	12.3± 6.2	12.3± 6.2	12.3± 6.2	12.3± 6.2
10	12.1± 5.7	9.6± 3.0	8.2± 2.1	7.8± 2.0	7.8± 2.0	7.8± 2.0
15	11.2± 5.0	8.8± 2.5	7.1± 1.7	6.6± 1.5	6.3± 1.4	6.4± 1.4
20	10.8± 4.6	7.9± 2.1	6.7± 1.5	6.2± 1.3	5.9± 1.2	6.0± 1.2
30	11.0± 4.7	7.1± 1.8	6.0± 1.3	5.6± 1.1	5.2± 0.9	4.9± 0.9

Table 28: $\langle {P_t}^{\gamma+Jet} \rangle\ (GeV/c)$

$P_{t\ cut}^{\ clust}$ (GeV/c)	$P_{t\ cut}^{\ out}\ (GeV/c)$					
	5	10	15	20	30	1000
5	4.1	4.5	4.7	4.7	4.7	4.7
10	4.5	5.4	6.0	6.2	6.4	6.4
15	4.4	5.5	6.4	7.1	7.4	7.4
20	4.3	5.5	6.4	7.4	8.0	8.0
30	4.3	5.5	6.6	7.7	9.2	10.0

Table 29: $\langle F \rangle,\ F = ({P_t}^{\gamma} - {P_t}^{Jet})/{P_t}^{\gamma}$

$P_{t\ cut}^{\ clust}$ (GeV/c)	$P_{t\ cut}^{\ out}\ (GeV/c)$					
	5	10	15	20	30	1000
5	-0.004	-0.009	-0.007	-0.007	-0.007	-0.007
10	-0.009	-0.015	-0.018	-0.022	-0.023	-0.023
15	-0.007	-0.013	-0.015	-0.021	-0.027	-0.027
20	-0.006	-0.011	-0.013	-0.017	-0.021	-0.021
30	-0.006	-0.012	-0.012	-0.016	-0.025	-0.033

Table 30: $\sigma(F),\ F = ({P_t}^{\gamma} - {P_t}^{Jet})/{P_t}^{\gamma}$

$P_{t\ cut}^{\ clust}$ (GeV/c)	$P_{t\ cut}^{\ out}\ (GeV/c)$					
	5	10	15	20	30	1000
5	0.073	0.080	0.082	0.082	0.082	0.082
10	0.073	0.086	0.090	0.096	0.096	0.096
15	0.074	0.088	0.098	0.115	0.119	0.119
20	0.073	0.087	0.098	0.120	0.131	0.131
30	0.072	0.089	0.102	0.129	0.153	0.158

$$\hat{p}_{\perp}^{min} = 100\ GeV/c, \quad \epsilon^{jet} < 2\%.$$

Table 31: Number of events per $L_{int} = 3\ fb^{-1}$

$P_{t\ cut}^{clust}$ (GeV/c)	$P_{t\ cut}^{out}\ (GeV/c)$					
	5	10	15	20	30	1000
5	9900	15600	16900	17000	17000	17000
10	22700	47400	57700	60400	61500	61500
15	26600	59500	77700	86400	92100	92600
20	27800	63100	86100	99700	112600	114500
30	28300	65500	91600	108700	134200	144300

Table 32: S/B

$P_{t\ cut}^{clust}$ (GeV/c)	$P_{t\ cut}^{out}\ (GeV/c)$					
	5	10	15	20	30	1000
5	58.6±45.2	56.8±34.4	55.8±32.2	56.0±32.3	56.0±32.3	56.0±32.3
10	30.6±11.8	30.8± 8.4	26.7± 5.7	27.9± 6.0	27.3± 5.8	27.3± 5.8
15	32.8±12.0	26.5± 6.0	21.2± 3.8	22.2± 3.9	20.8± 3.4	21.1± 3.4
20	29.0± 9.9	21.6± 4.3	17.2± 2.7	17.8± 2.7	15.5± 2.1	15.7± 2.1
30	27.4± 9.1	19.7± 3.8	16.2± 2.4	15.4± 2.1	12.2± 1.4	11.5± 1.2

Table 33: $\langle {P_t}^{\gamma+Jet} \rangle\ (GeV/c)$

$P_{t\ cut}^{clust}$ (GeV/c)	$P_{t\ cut}^{out}\ (GeV/c)$					
	5	10	15	20	30	1000
5	3.5	4.5	5.0	5.0	5.0	5.0
10	3.9	5.3	6.4	6.8	7.0	7.0
15	4.1	5.7	7.1	8.1	8.9	9.0
20	4.3	5.9	7.5	8.7	10.2	10.6
30	4.3	5.9	7.7	9.1	11.8	13.4

Table 34: $\langle F \rangle,\ F = ({P_t}^{\gamma} - {P_t}^{Jet})/{P_t}^{\gamma}$

$P_{t\ cut}^{clust}$ (GeV/c)	$P_{t\ cut}^{out}\ (GeV/c)$					
	5	10	15	20	30	1000
5	0.000	-0.002	-0.001	-0.002	-0.002	-0.002
10	0.001	0.000	-0.002	-0.002	-0.002	-0.002
15	0.001	-0.001	-0.003	-0.003	-0.002	-0.003
20	0.001	-0.001	-0.004	-0.003	-0.002	-0.003
30	0.001	-0.002	-0.004	-0.004	-0.004	-0.004

Table 35: $\sigma(F),\ F = ({P_t}^{\gamma} - {P_t}^{Jet})/{P_t}^{\gamma}$

$P_{t\ cut}^{clust}$ (GeV/c)	$P_{t\ cut}^{out}\ (GeV/c)$					
	5	10	15	20	30	1000
5	0.025	0.033	0.035	0.035	0.035	0.035
10	0.026	0.036	0.042	0.044	0.046	0.046
15	0.027	0.037	0.045	0.052	0.056	0.057
20	0.028	0.038	0.046	0.056	0.064	0.067
30	0.028	0.038	0.047	0.059	0.076	0.086

$$\hat{p}_{\perp}^{min} = 200\ GeV/c, \quad \epsilon^{jet} < 2\%.$$

Table 36: Number of events per $L_{int} = 3\ fb^{-1}$

$P_{t\ cut}^{clust}$ (GeV/c)	$P_{t\ cut}^{out}\ (GeV/c)$					
	5	10	15	20	30	1000
5	540	1000	1090	1120	1120	1130
10	1380	3260	4130	4480	4550	4560
15	1710	4200	5980	6900	7410	7460
20	1800	4570	6730	8150	9340	9650
30	1840	4770	7200	8970	11240	12680

Table 37: S/B

$P_{t\ cut}^{clust}$ (GeV/c)	$P_{t\ cut}^{out}\ (GeV/c)$					
	5	10	15	20	30	1000
5	104 ± 104	177 ± 167	114 ± 84	116 ± 85	116 ± 85	116 ± 85
10	45.6±20.0	51.6±14.9	45.4±11.2	41.7± 9.7	41.7± 9.7	42.4± 9.7
15	39.8±14.8	45.6±11.5	41.5± 8.4	33.8± 5.8	30.4± 4.9	30.0± 4.8
20	34.8±11.9	40.0± 9.1	33.1± 5.7	27.9± 4.1	23.2± 3.0	21.4± 2.6
30	35.7±12.2	33.2± 6.9	27.3± 4.2	22.9± 3.0	19.1± 2.1	16.4± 1.6

Table 38: $\langle {P_t}^{\gamma+Jet} \rangle\ (GeV/c)$

$P_{t\ cut}^{clust}$ (GeV/c)	$P_{t\ cut}^{out}\ (GeV/c)$					
	5	10	15	20	30	1000
5	4.0	4.8	5.3	5.4	5.5	5.8
10	4.5	5.9	6.9	7.6	7.8	7.9
15	4.6	6.1	7.7	8.9	9.8	10.0
20	4.7	6.3	8.0	9.5	11.2	12.0
30	4.7	6.3	8.2	9.9	12.8	15.7

Table 39: $\langle F \rangle,\ F = ({P_t}^{\gamma} - {P_t}^{Jet})/{P_t}^{\gamma}$

$P_{t\ cut}^{clust}$ (GeV/c)	$P_{t\ cut}^{out}\ (GeV/c)$					
	5	10	15	20	30	1000
5	0.003	0.002	0.003	0.003	0.003	0.003
10	0.001	0.002	0.003	0.003	0.003	0.003
15	0.001	0.002	0.004	0.004	0.004	0.004
20	0.001	0.002	0.003	0.004	0.003	0.003
30	0.001	0.002	0.003	0.004	0.003	0.002

Table 40: $\sigma(F),\ F = ({P_t}^{\gamma} - {P_t}^{Jet})/{P_t}^{\gamma}$

$P_{t\ cut}^{clust}$ (GeV/c)	$P_{t\ cut}^{out}\ (GeV/c)$					
	5	10	15	20	30	1000
5	0.015	0.018	0.020	0.021	0.022	0.023
10	0.016	0.020	0.023	0.026	0.027	0.027
15	0.016	0.021	0.026	0.030	0.033	0.034
20	0.016	0.021	0.027	0.031	0.038	0.041
30	0.016	0.021	0.027	0.033	0.043	0.050